Journal of Solid Mechanics Vol. 10, No. 3 (2018) pp. 489-501

Influences of Small-Scale Effect and Boundary Conditions on the Free Vibration of Nano-Plates: A Molecular Dynamics Simulation

S.F. Asbaghian Namin, R. Pilafkan *

University of Mohaghegh Ardabili, Ardabil, Iran

Received 28 May 2018; accepted 2 July 2018

ABSTRACT

This paper addresses the influence of boundary conditions and small-scale effect on the free vibration of nano-plates using molecular dynamics (MD) and nonlocal elasticity theory. Based on the MD simulations, Large-scale Atomic/Molecular Massively Parallel Simulator (LAMMPS) is used to obtain fundamental frequencies of single layered graphene sheets (SLGSs) which modeled in this paper as the most common nano-plates. On the other hand, governing equations are derived using nonlocal elasticity and the first-order shear deformation theory (FSDT). Afterwards, these equations solved using generalized differential quadrature method (GDQ). The small-scale effect is applied in the governing equations of motion by nonlocal parameter. The effects of different side lengths, boundary conditions, and nonlocal parameter are inspected for the aforementioned methods. The results obtained from the MD simulations are compared with those of nonlocal elasticity theory to calculate appropriate values for the nonlocal parameter. As a result, for the first time, the nonlocal parameter values are suggested for graphene sheets with various boundary conditions. Furthermore, it is shown that nonlocal elasticity approach using classical plate theory (CLPT) assumptions overestimates the natural frequencies.

Keywords : Nano-plates; Molecular dynamics simulations; Fundamental frequencies; Nonlocal elasticity theory; Nonlocal parameter.

1 INTRODUCTION

AFTER the synthesis and characterization of carbon nanotubes by Iijima in 1991 experimental and theoretical studies in the fields of microstructures and nanostructures increased substantially [1]. Eventually with the development of these fields, nano-plates, including graphene sheets, drew attentions to themselves, because of their unique mechanical, electrical, and electronic properties. Nowadays, graphene sheets are widely used in nano-sensors, nano-oscillators, electrical batteries, nanocomposites and nano-electromechanical resonators [2-4]. As a result, investigating the mechanical characteristics of nano-plates, especially graphene sheets, is inevitable.

Since the applicability of classical field theories is correlated with length scales, for accurate prediction of the mechanical behavior of nanomaterials the small scale effect must be taken into account. Therefore, local continuum modeling can successfully explain and predict physical phenomena at the macro-scale level; nevertheless, its

*Corresponding author.
E-mail address: rezapilafkan@um.ac.ir (R.Pilafkan).

application in nano-scale remains questionable. As a result, usually, the nonlocal elasticity theory is used in modeling structures at nano-scale instead of classical elasticity theory [4].

Among various mechanical characteristics of nano-plates, their vibrational behavior is of great importance. Due to difficulties in conducting experiments to determine the mechanical properties of nano-plates, generally analytical methods, numerical modelings, and molecular dynamics simulations are used to determine their vibrational characteristics. Up until now, several studies have been done on the vibration of nanostructures and specifically nano-plates. Murmu and Pradhan [2] employed an analytical method using the separation of variables to investigate the effect of nonlocal parameter on the vibration of graphene sheets. Pradhan and Phadikar [5] calculated natural frequencies of graphene sheets analytically by modifying classical laminated plate theory (CLPT) and first shear deformation theory (FSDT) using nonlocal elasticity theory. Hosseini-Hashemi et al. [6] used Mindlin theory and introduced some potential and auxiliary functions to study the free vibration of graphene sheets. Zhang et al. [7] implemented an element-free kp-Ritz to investigate the free vibrational behavior of a single-layered graphene sheet. Moreover, Zhang et al. [8] used nonlocal elasticity theory and CLPT to study the vibrational behavior of bilayer graphene sheets (BLGSs) in a magnetic field.

Ansari et al. [9] implemented the finite element method (FEM) to analyze the free vibration of multi-layered graphene sheets. Ansari et al. [10] investigated the vibration of single-layered graphene sheets (SLGSs) using a nonlocal continuum plate model and then validated the calculated results with ones obtained by the molecular dynamics simulations. They calculated nonlocal parameters by comparing results obtained from two aforementioned methods. The MD simulations are performed using NanoHive, a MD simulator, but unfortunately NanoHive currently is not available and no longer supported by its creators. Hence, utilizing other programs is seemed necessary. Pradhan and Kumar [11] studied the small-scale effect on the vibration analysis of orthotropic SLGSs. They employed the differential quadrature method (DQM) to solve governing equations derived using the nonlocal elasticity theory. Xing and Liu [12] found exact solutions for the free vibration of thin orthotropic rectangular plates. This problem solved for various boundary conditions and validated with results obtained by FEM. Setoodeh et al. [13] investigated the free vibration analysis of orthotropic SLGSs using nonlocal Mindlin plate theory and employing DQM. Shahidi et al. [14] investigated the vibration of orthotropic triangular nano-plates using nonlocal elasticity theory and Galerkin Method. Finally, Zhang et al. [15] modeled the nonlinear vibrational behavior of graphene sheets using CLPT and nonlocal elasticity theory.

Although the results which calculated by the nonlocal elasticity theory change significantly by the nonlocal parameter, only little data provided for the correct values of this parameter in the literature. Most papers concentrated on the impact of changing the nonlocal parameter on natural frequencies rather than calculating the accurate values of them.

Hence, the free vibrations of SLGSs, therefore, are investigated in present work using nonlocal elasticity theory and the MD simulation approach. Although SLGSs have an orthotropic nature, their mechanical properties in the FSDT equations are considered isotropic. However, this assumption may cause a slight error in the final results obtained by nonlocal elasticity theory. A nonlocal FSDT applied in which the effects of rotary inertia and transverse shear are included. Natural frequencies are obtained for various boundary conditions. The LAMMPS program is utilized to conduct the MD simulations for investigating the vibrational behavior of SLGSs. Results obtained from these two methods are compared with each other to find proper values for nonlocal parameters. Finally, for the first time, the appropriate values of nonlocal parameters are proposed for the vibration of SLGSs with various boundary conditions.

2 NONLOCAL PLATE GOVERNING EQUATIONS

As mentioned in previous section in this paper, the nonlocal elasticity theory is commonly used in modeling the nanostructures rather than classical elasticity theory. Based on nonlocal elasticity theory, stress at any point in a continuum is a function of strain at all points of the continuum [16]. Accordingly, the constitutive relation in the small scales is written as follows [5]:

$$(1-\mu\nabla^2)\sigma = t \tag{1}$$

where σ is nonlocal stress tensor, t is local stress tensor, and μ denotes the nonlocal parameter. Using (1) and based on FSDT, one can obtain a relation between the nonlocal stresses and strains for an isotropic plate [17]:

$$\begin{Bmatrix}\sigma_{xx}\\ \sigma_{yy}\\ \sigma_{xy}\end{Bmatrix}-\mu\nabla^2\begin{Bmatrix}\sigma_{xx}\\ \sigma_{yy}\\ \sigma_{xy}\end{Bmatrix}=\begin{bmatrix}E/(1-\upsilon^2) & \upsilon E/(1-\upsilon^2) & 0\\ \upsilon E/(1-\upsilon^2) & E/(1-\upsilon^2) & 0\\ 0 & 0 & 2G\end{bmatrix}\begin{Bmatrix}\varepsilon_{xx}\\ \varepsilon_{yy}\\ \varepsilon_{xy}\end{Bmatrix} \tag{2}$$

$$\begin{Bmatrix}\sigma_{xz}\\ \sigma_{yz}\end{Bmatrix}-\mu\nabla^2\begin{Bmatrix}\sigma_{xz}\\ \sigma_{yz}\end{Bmatrix}=\begin{bmatrix}2G & 0\\ 0 & 2G\end{bmatrix}\begin{Bmatrix}\varepsilon_{xz}\\ \varepsilon_{yz}\end{Bmatrix} \tag{3}$$

where E,G and υ are the young modulus, the shear modulus, and the poisson's ratio, respectively. Furthermore, FSDT is used in order to establish governing equations. In this theory, both shear deformations and rotational inertia are taken into account. As a result, despite CLPT, transverse normals (i.e., straight lines perpendicular to the mid-surface) do not remain perpendicular to the mid-surface after deformation [18]. Fig. 1 shows the coordinate system for the SLGS. As shown in the figure, $z=0$ plane is the middle plane of the SLGS. Considering FSDT, displacement field for the plate can be expressed as [18]:

$$u_x(x,y,z,t)=u(x,y,t)+z\psi_x(x,y,t) \tag{4}$$

$$u_y(x,y,z,t)=v(x,y,t)+z\psi_y(x,y,t) \tag{5}$$

$$u_z(x,y,z,t)=w(x,y,t) \tag{6}$$

where u_x, u_y, and u_z are displacements of an arbitrary point on $z=0$ plane in x, y, and z directions and u, v, and w are displacements of an arbitrary point (x,y,z) in x, y, and z directions, respectively. Additionally, ψ_x and ψ_y are rotations about x and y axis, respectively.

Using (4)-(6) the strains are obtained as follows [18]:

$$\begin{Bmatrix}\varepsilon_{xx}\\ \varepsilon_{yy}\\ \varepsilon_{xy}\end{Bmatrix}=\begin{Bmatrix}\dfrac{\partial u}{\partial x}\\ \dfrac{\partial v}{\partial y}\\ \dfrac{1}{2}\left(\dfrac{\partial u}{\partial y}+\dfrac{\partial v}{\partial x}\right)\end{Bmatrix}+z\begin{Bmatrix}\dfrac{\partial \psi_x}{\partial x}\\ \dfrac{\partial \psi_y}{\partial y}\\ \dfrac{1}{2}\left(\dfrac{\partial \psi_x}{\partial x}+\dfrac{\partial \psi_y}{\partial y}\right)\end{Bmatrix} \tag{7}$$

$$\begin{Bmatrix}\varepsilon_{xz}\\ \varepsilon_{yz}\end{Bmatrix}=\begin{Bmatrix}\dfrac{1}{2}\left(\psi_x+\dfrac{\partial w}{\partial x}\right)\\ \dfrac{1}{2}\left(\psi_y+\dfrac{\partial w}{\partial y}\right)\end{Bmatrix} \tag{8}$$

ε_{xx}, ε_{yy}, and ε_{zz} and ε_{xy}, ε_{xz}, and ε_{yz} denote normal and shear strain tensor components, respectively. It should be noted that $\varepsilon_{zz}=0$, because it was assumed that the transverse normals are inextensible.

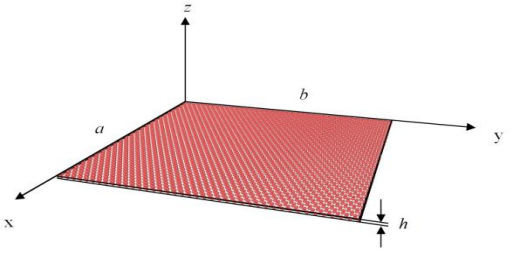

Fig.1
Coordinate system for SLGS.

On the other hand, the principle of virtual work can be applied to derive the equilibrium equations of the SLGS [5]. Following governing equations are obtained, using the principle of virtual work [5]:

$$\frac{\partial N_{xx}}{\partial x}+\frac{\partial N_{xy}}{\partial y}=I_1\frac{\partial^2 u}{\partial t^2} \tag{9}$$

$$\frac{\partial N_{xy}}{\partial x}+\frac{\partial N_{yy}}{\partial y}=I_1\frac{\partial^2 v}{\partial t^2} \tag{10}$$

$$\frac{\partial Q_{xx}}{\partial x}+\frac{\partial Q_{yy}}{\partial y}+q+\{\frac{\partial}{\partial x}(N_{xx}\frac{\partial w}{\partial x})+\frac{\partial}{\partial y}(N_{yy}\frac{\partial w}{\partial y})+\frac{\partial}{\partial x}(N_{xy}\frac{\partial w}{\partial y})+\frac{\partial}{\partial y}(N_{xy}\frac{\partial w}{\partial x})\}=I_1\frac{\partial^2 w}{\partial t^2} \tag{11}$$

$$\frac{\partial M_{xx}}{\partial x}+\frac{\partial M_{xy}}{\partial y}-Q_{xx}=I_3\frac{\partial^2 \psi_x}{\partial t^2} \tag{12}$$

$$\frac{\partial M_{xy}}{\partial x}+\frac{\partial M_{yy}}{\partial y}-Q_{yy}=I_3\frac{\partial^2 \psi_y}{\partial t^2} \tag{13}$$

where N_{xx}, N_{xy}, N_{yy}, M_{xx}, M_{xy}, M_{yy}, Q_{xx}, and Q_{yy} denote stress resultants, which are defined as follows:

$$N_{xx}=\int_{-h/2}^{h/2}\sigma_{xx}dz\,,\ N_{xy}=\int_{-h/2}^{h/2}\sigma_{xy}dz\,,\ N_{yy}=\int_{-h/2}^{h/2}\sigma_{yy}dz \tag{14}$$

$$\begin{aligned}&M_{xx}=\int_{-h/2}^{h/2}z\,\sigma_{xx}dz\,,\ M_{xy}=\int_{-h/2}^{h/2}z\,\sigma_{xy}dz\,,\\&M_{yy}=\int_{-h/2}^{h/2}z\,\sigma_{yy}dz\end{aligned} \tag{15}$$

$$Q_{xx}=\int_{-h/2}^{h/2}\sigma_{xz}dz\,,\ Q_{yz}=\int_{-h/2}^{h/2}\sigma_{yz}dz \tag{16}$$

Furthermore, I_1 and I_3 are mass moments of inertia and defined as:

$$I_1=\int_{-h/2}^{h/2}\rho dz\,,\ I_3=\int_{-h/2}^{h/2}\rho h^2 dz \tag{17}$$

Subsequently, (2), (3), (7), (8), and (14) -(16) can be used to express stress resultants in terms of the displacements:

$$M_{xx}-\mu\nabla^2 M_{xx}=D(\frac{\partial \psi_x}{\partial x}+\upsilon\frac{\partial \psi_y}{\partial y}) \tag{18}$$

$$M_{yy} - \mu\nabla^2 M_{yy} = D(\frac{\partial \psi_y}{\partial y} + \upsilon \frac{\partial \psi_x}{\partial x}) \tag{19}$$

$$M_{xy} - \mu\nabla^2 M_{xy} = \frac{1}{2}(1-\upsilon)D(\frac{\partial \psi_x}{\partial y} + \frac{\partial \psi_y}{\partial x}) \tag{20}$$

$$Q_{xx} - \mu\nabla^2 Q_{xx} = kGh(\frac{\partial w}{\partial x} + \psi_x) \tag{21}$$

$$Q_{yy} - \mu\nabla^2 Q_{yy} = kGh(\frac{\partial w}{\partial y} + \psi_y) \tag{22}$$

In these relations $k = 5/6$ is the shear correction factor. Finally, using (18)-(22), (11)-(13) expressed in the terms of displacements:

$$kGh(\frac{\partial \psi_x}{\partial x} + \frac{\partial \psi_y}{\partial y} + \frac{\partial^2 w}{\partial x^2} + \frac{\partial^2 w}{\partial y^2}) = I_1(\frac{\partial^2 w}{\partial t^2} - \mu\nabla^2 \frac{\partial^2 w}{\partial t^2}) \tag{23}$$

$$D\frac{\partial^2 \psi_x}{\partial x^2} + \frac{(1+\upsilon)}{2}D\frac{\partial^2 \psi_y}{\partial x \partial y} + \frac{1}{2}(1-\upsilon)D\frac{\partial^2 \psi_x}{\partial y^2} - kGh(\frac{\partial w}{\partial x} + \psi_x) = I_3(\frac{\partial^2 \psi_x}{\partial t^2} - \mu\nabla^2 \frac{\partial^2 \psi_x}{\partial t^2}) \tag{24}$$

$$\frac{(1+\upsilon)}{2}D\frac{\partial^2 \psi_x}{\partial x \partial y} + D\frac{\partial^2 \psi_y}{\partial y^2} + \frac{1}{2}(1-\upsilon)D\frac{\partial^2 \psi_y}{\partial x^2} - kGh(\frac{\partial w}{\partial y} + \psi_y) = I_3(\frac{\partial^2 \psi_y}{\partial t^2} - \mu\nabla^2 \frac{\partial^2 \psi_y}{\partial t^2}) \tag{25}$$

It should be mentioned that (9), (10) and the terms including q, N_{xx}, N_{xy}, and N_{yy} were eliminated, because it was assumed that the plate is free from any in-plane or transverse loading [5].

3 DIFFERENTIAL QUADRATURE METHOD

Generalized differential quadrature method is a numerical solution technique for solving initial and boundary condition problems of various engineering applications. It can be used as a convenient alternative to the finite difference and finite element methods due to its great accuracy and capability in solving complicated ordinary and partial differential equations [19]. In summary, in this method N_x and N_y grid points are chosen in x and y directions, then partial derivative of a function with respect to a coordinate (x or y) at a grid point is estimated by weighted linear sum of values of that function in all grid points along that direction. Therefore, *rth* derivative of function $\varphi(x, y)$ at point $x = x_i$ and in direction $y = y_j$ can be obtained using the following relation:

$$\left.\frac{\partial^r \varphi}{\partial x^r}\right|_{x=x_i} = \sum_{k=1}^{N_x} A_{ik}^{(r)} \varphi_{kj} \tag{26}$$

Similarly, one can write:

$$\left.\frac{\partial^s \varphi}{\partial y^s}\right|_{y=y_i} = \sum_{l=1}^{N_y} B_{jm}^{(s)} \varphi_{im} \tag{27}$$

where $A_{ik}^{(r)}$ and $B_{jm}^{(s)}$ are weighting coefficients and $\varphi_{ij}=\varphi\left(x_i,y_j\right)$. The weighting coefficients of the first derivatives are obtained from:

$$A_{ik}^{(1)}=\frac{\prod_{v=1,v\neq i}^{N_x}\left(x_i-x_v\right)}{\left(x_i-x_k\right)\prod_{v=1,v\neq k}^{N_x}\left(x_k-x_v\right)};\ k,i=1,...,N_x,\ k\neq i \tag{28}$$

Furthermore, the weighting coefficients of higher-order derivatives are determined by:

$$A_{ik}^{(r)}=\begin{cases} r\left[A_{ii}^{(r-1)}A_{ik}^{(1)}-\dfrac{A_{ik}^{(r-1)}}{x_i-x_k}\right], & i\neq k \\ A_{ii}^{(r)}=-\sum_{v=1,v\neq i}^{N_x}A_{iv}^{(r)}, & i=k \end{cases} \tag{29}$$
$$(i,j=1,2,3,...,N_x;\ 2\le r\le N_x-1)$$

To solve (23) -(25) using GDQ technique, these equations should be rewritten in GDQ form. Since w, ψ_x, and ψ_y were assumed as the periodic functions, one can write:

$$x=aX,\ y=bY \tag{30}$$

$$w=hWe^{j\omega t},\ \psi_x=\Psi_x e^{j\omega t},\ \psi_y=\Psi_y e^{j\omega t} \tag{31}$$

Eventually, using (26) -(29) and substituting (30) and (31) in (23) -(25) the following analogous equations can be obtained:

$$kGh\left(\frac{h}{a^2}\sum_{k=1}^{N_x}A_{ik}^{(2)}W_{kj}+\frac{1}{a}\sum_{k=1}^{N_x}A_{ik}^{(1)}\Psi_{x_{kj}}+\frac{h}{b^2}\sum_{m=1}^{N_y}B_{jm}^{(2)}W_{im}+\frac{1}{b}\sum_{m=1}^{N_y}B_{jm}^{(1)}\Psi_{y_{im}}\right)=-\omega^2[I]W_{ij}-\mu I_1\left(\frac{1}{a^2}\sum_{k=1}^{N_x}A_{ik}^{(2)}W_{kj}+\frac{1}{b^2}\sum_{m=1}^{N_y}B_{jm}^{(2)}W_{im}\right)] \tag{32}$$

$$\frac{D}{a^2}\sum_{k=1}^{N_x}A_{ik}^{(2)}\Psi_{x_{kj}}+\frac{(1+\upsilon)}{2}\frac{D}{ab}\sum_{k=1}^{N_x}\sum_{m=1}^{N_y}A_{ik}^{(2)}B_{jm}^{(2)}\Psi_{y_{km}}+\frac{1}{2}(1-\upsilon)\frac{D}{b^2}\sum_{m=1}^{N_y}B_{jm}^{(2)}\Psi_{x_{im}}=-\omega^2[I_3W_{ij}-\mu I_3\left(\frac{1}{a^2}\sum_{k=1}^{N_x}A_{ik}^{(2)}\Psi_{x_{kj}}+\frac{1}{b^2}\sum_{m=1}^{N_y}B_{jm}^{(2)}\Psi_{x_{im}}\right)] \tag{33}$$

$$\frac{D}{b^2}\sum_{m=1}^{N_y}B_{jm}^{(1)}\Psi_{y_{im}}+\frac{(1+\upsilon)}{2}\frac{D}{ab}\sum_{k=1}^{N_x}\sum_{m=1}^{N_y}A_{ik}^{(2)}B_{jm}^{(2)}\Psi_{x_{km}}+\frac{1}{2}(1-\upsilon)\frac{D}{a^2}\sum_{k=1}^{N_x}A_{ik}^{(2)}\Psi_{y_{kj}}=-\omega^2[I_3W_{ij}-\mu I_3\left(\frac{1}{a^2}\sum_{k=1}^{N_x}A_{ik}^{(2)}\Psi_{y_{kj}}+\frac{1}{b^2}\sum_{m=1}^{N_y}B_{jm}^{(2)}\Psi_{y_{im}}\right)]; \tag{34}$$
$$i=1,2,...,N_x,\ j=1,2,...,N_y$$

In order to solve equation, applying the appropriate boundary conditions is necessary. For the all edges clamped (CCCC) boundary conditions, in which (C) refers to the clamped boundary conditions one can write:

$$\begin{aligned} &X=0,1;\ W=\Psi_x=\Psi_y=0 \\ &Y=0,1;\ W=\Psi_x=\Psi_y=0 \end{aligned} \tag{35}$$

The GDQ form of boundary conditions:

$$\begin{aligned} &i = 1, N_x;\ W_{ij} = \Psi_{x_{ij}} = \Psi_{y_{ij}} = 0 \\ &j = 1, N_y;\ W_{ij} = \Psi_{x_{ij}} = \Psi_{y_{ij}} = 0 \end{aligned} \tag{36}$$

For the all edges simply supported (SSSS) boundary conditions, in which (S) refers to the simply supported boundary conditions the following relations applied:

$$\begin{aligned} &X = 0,1;\ W = \Psi_y = 0,\ M_{xx} = 0 \\ &Y = 0,1;\ W = \Psi_x = 0,\ M_{yy} = 0 \end{aligned} \tag{37}$$

The GDQ form of boundary conditions:

$$\begin{aligned} &i = 1, N_x;\ W_{ij} = \Psi_{y_{ij}} = 0; \\ &D\sum_{k=1}^{N_x} A_{ik}^{(1)} \Psi_{x_{kj}} + \upsilon D \sum_{m=1}^{N_y} B_{jm}^{(1)} \Psi_{y_{im}} = 0 \\ &j = 1, N_y;\ W_{ij} = \Psi_{x_{ij}} = 0; \\ &\upsilon D\sum_{k=1}^{N_x} A_{ik}^{(1)} \Psi_{x_{kj}} + D \sum_{m=1}^{N_y} B_{jm}^{(1)} \Psi_{y_{im}} = 0 \end{aligned} \tag{38}$$

Accordingly, GDQ form of SCSC boundary conditions can be obtained by using clamped boundary conditions at $x = 0, a$ and simply supported boundary conditions at $y = 0, b$.

Assembling (32)-(38) into an eigenvalue problem is the final step in the GDQ solution procedure. This eigenvalue problem can be written as following matrix form:

$$\begin{bmatrix} [S_{dd}] & [S_{db}] \\ [S_{bd}] & [S_{bb}] \end{bmatrix}_{(N \times N)} \begin{Bmatrix} \delta_d \\ \delta_b \end{Bmatrix}_{(N)} = \begin{Bmatrix} \{\omega^2 [M_{dd}] \{\delta_d\}\} \\ \{0\} \end{Bmatrix}_{(N)} \tag{39}$$

where $[S_{dd}]$, $[S_{db}]$, $[S_{bd}]$, and $[S_{bb}]$ are the coefficient matrices of the left hand side of (32)-(34) in which the subscript b and d refer to the boundary and domain, respectively. $[M_{dd}]$ is the coefficient matrix of the right hand side of (32)-(34). $\{\delta_d\}$ and $\{\delta_b\}$ are the displacement vectors corresponding to the domain and boundary grid points. Eigenvalues (i.e. natural frequencies, ω) and eigenvectors of (39) are calculated using the condensation technique as follows [10]:

$$\left[M_{dd}^{-1}\right]\left([S_{dd}] - [S_{db}]\left[S_{bb}^{-1}\right][S_{bd}]\right)\{\delta_d\} - \omega^2 [I][\delta_d] = 0 \tag{40}$$

4 MOLECULAR DYNAMICS SIMULATION

Molecular dynamic (MD) is a commonly used computational tool for simulating the properties of liquids and solids that has wide applications in analysis of nanostructures [20]. The essence of molecular dynamics is solving *N*-body problem numerically using classical mechanics (i.e. Newton's Laws of Motion) [21]. Each of bodies (e.g. particles, molecules and etc.) in the simulation is treated as a point mass and Newton's equations are integrated to compute their motion. From the motion of the ensemble of atoms a variety of useful microscopic and macroscopic information can be extracted including but not limited to structural properties. The physics of the model is contained in a potential energy function for the system, from which individual force equations for each atom are derived [20].

Since MD simulations are related to interatomic and intermolecular interactions, they can be employed to investigate larger systems and can give accurate results through the use of suitable and accurate potential functions [10].

Among Several free and non-free programs that are available for the molecular dynamics simulations, LAMMPS was chosen for this work. It is a classical molecular dynamics code that models an ensemble of particles in a liquid, solid, or gaseous state. Although it was designed for parallel computers, it runs efficiently on single-processor desktop or laptop machines [22].

As mentioned earlier in this section the potential function plays an important role in obtaining accurate and reliable results. Before the simulation, a suitable potential function should be selected among various choices. In this paper, Adaptive Intermolecular Reactive Empirical Bond Order (AIREBO) potential function was chosen that is used widely in simulation of hydrocarbon molecules and gives more accurate results than the Tersoff potential function [23]. In order to perform MD simulation, the SLGS should be modeled in the first place. All simulations performed for the zigzag graphene sheets. Different kinds of graphene sheets conformation are shown in Fig. 2. One or four layers of atoms at edges were fixed to apply the simply supported or clamped boundary conditions, respectively. Also, the NVT ensemble was chosen as a thermostat to maintain the temperature of system.

After initial settings, the SLGS was simulated to obtain the fundamental frequency. To achieve this goal midpoint of graphene sheet was dragged vertically and then released to initiate the first mode of the free vibrations for 2000000 time steps of 1 *fs*. The displacement-time curve of midpoint was obtained from LAMMPS outputs. Finally, the fundamental frequency was calculated using fast Fourier transform (FFT) algorithm. It takes displacements over time and eliminates possible noise frequencies to obtain the fundamental frequencies of the free vibration. The FFTs output is a curve, with several peaks. The frequencies corresponded to the first, second and ... peaks represent the first, second and ... natural frequencies [24].

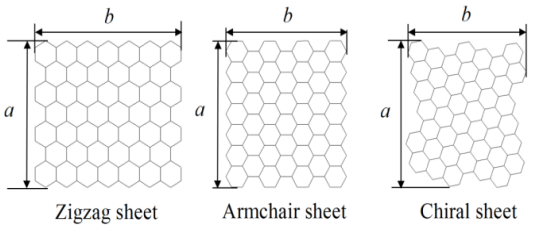

Fig.2
Chirality and geometrical parameters of single-layered graphene sheets. [25]

5 RESULTS AND DISCUSSION

The mechanical properties of graphene sheets used in this work are presented in Table 1. for isotropic graphene sheets. Also, the thickness of each plate and the density of graphene are assumed $h = 0.34\ (nm)$ and $\rho = 2300\ (kg/m^3)$. The convergence study for the GDQ technique is conducted first. To achieve this goal, the fundamental frequency is calculated for a square SLGS with side length of 10 nm and SSSS boundary conditions for both local $(\mu = 0)$ and nonlocal $(\mu = 1\ (nm)^2)$ assumptions. Table 2. shows the fundamental frequencies for various number of grid points chosen along each axis. It can be noted from Table 2. that after employing 11 grid points results converge and there is no need for further increasing in the number of grid points.

Subsequently, the natural frequencies obtained in present work using the GDQ method for both local and nonlocal plate are listed in Table 3. and compared with exact solutions [5]. They are acquired for a square isotropic SLGS with 10 *nm* side length and all edges simply supported boundary conditions. From this table, one could find that present results are in good agreement with those of the exact solution [5].

Table 1
Mechanical properties of isotropic graphene sheets.

$E\ (Tpa)$	υ	$G\ (Tpa)$
1.02	0.3	0.392

Table 2
Convergence study of fundamental frequencies (THz) for the GDQ method.

Number of grid points	local ($\mu = 0$)	nonlocal ($\mu = 1$)
7	0.0679	0.0620
9	0.0678	0.0619
11	0.0678	0.0619
13	0.0678	0.0619
15	0.0678	0.0619

Table 3
Comparison of natural frequencies (THz) using the GDQ method with the exact solution.

	local			nonlocal		
Mode number	GDQ	Exact (CLPT[5])[1]	Exact (FSDT[5])	GDQ	Exact (CLPT[5])[1]	Exact (FSDT[5])
1	0.0678	0.0680	0.0678	0.0619	0.0621	0.0620
2	0.1684	0.1698	0.1688	0.1375	0.1389	0.1381
3	0.1684	0.1698	0.1688	0.1375	0.1389	0.1381
4	0.2678	0.2712	0.2687	0.1996	0.2027	0.2009
5	0.3334	0.3387	0.3349	0.2356	0.2403	0.2376
6	0.3334	0.3387	0.3349	0.2356	0.2403	0.2376

[1] $\omega_{mn} = \sqrt{(D[(\frac{m\pi}{a})^2 + (\frac{n\pi}{b})^2]^2) / (\rho h + \frac{1}{12}\rho h^3[(\frac{m\pi}{a})^2 + (\frac{n\pi}{b})^2])(1 + \mu[(\frac{m\pi}{a})^2 + (\frac{n\pi}{b})^2])}$

Differences between these three solutions are indicated in Fig. 3 for the local plate. It is obvious that CLPT always overestimates the natural frequencies, as shown in the Fig. 3. Although the gap between the curves corresponding to CLPT and FSDT is significant for the side lengths smaller than 3 *nm*, this gap plunges evidently by increasing the side lengths. This is because CLPT is only accurate for thin plates. So when graphene sheet is not thin enough (i.e. $a/h \leq 50$) results using this theory can induce significant error.

The influence of the nonlocal parameter (μ) and the side length on the fundamental frequencies is investigated in Fig. 4 for the SSSS boundary conditions and Fig. 5 and Fig. 6 illustrate similar curves for the CCCC and SCSC boundary conditions, respectively. As shown in these figures, the fundamental frequency declines substantially with increase in the nonlocal parameter, for the side smaller than 30 *nm* because of the small-scale effect. However, for the larger SLGSs, nonlocal parameter has a negligible impact on the fundamental frequency, as expected. Therefore, the local forms of governing equations can be applied to the graphene sheets with larger sides without causing a noticeable error. Also, it can be observed that the lower fundamental frequency is obtained for the higher length of square. In addition, one can notice from these figures that increasing constraints results in higher natural frequencies. Thus, for the equal side lengths and nonlocal parameter values fundamental frequencies corresponding to CCCC boundaries are higher than those of SCSC boundaries and those of SCSC boundaries are higher than one's corresponding to the SSSS boundaries.

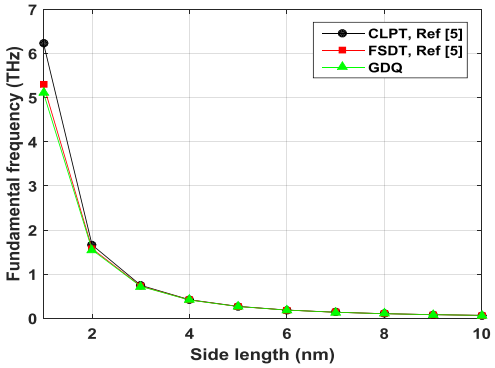

Fig.3
Comparison of reference [5] solutions with present work.

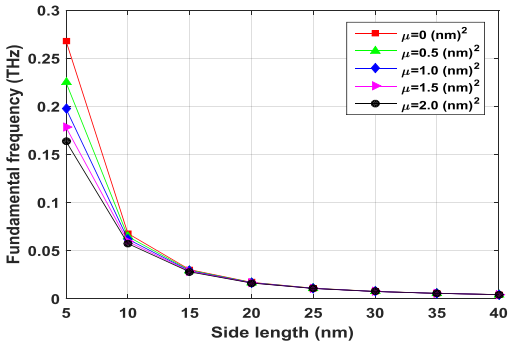

Fig.4
Effect of nonlocal parameter on the fundamental frequency for the SSSS boundary conditions.

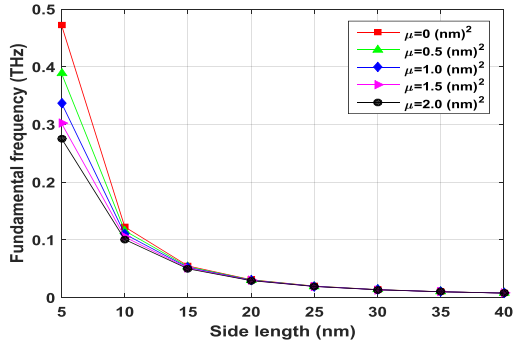

Fig.5
Effect of nonlocal parameter on the fundamental frequency for the CCCC boundary conditions.

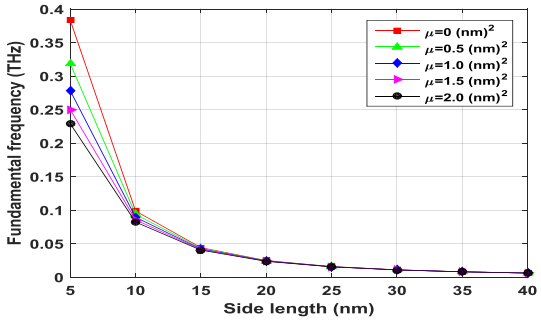

Fig.6
Effect of nonlocal parameter on the fundamental frequency for the SCSC boundary conditions.

As mentioned earlier, the nonlocal parameter plays an eminent role in the calculation of natural frequencies for a small graphene sheet (roughly, $a \le 30\ nm$)based on nonlocal elasticity theory. Hence, in order to implement the nonlocal elasticity theory, accurate determination of this parameter is inevitable. In this paper, molecular dynamics simulations are performed and obtained results are compared with those of the nonlocal elasticity to calculate the fundamental frequencies and evaluate the nonlocal parameter. Using aforementioned method, SLGS was excited to vibrate freely with first mode shape. Fig. 7 visualizes the excitation of the first mode shape in a square graphene. The fundamental frequencies of SLGSs with different boundary conditions and side lengths obtained using the MD simulations, are listed in Table 4.

Ansari et al. [10] proposed an optimization technique to determine the value of nonlocal parameter. In this method, the Euclidean norm of the difference between the fundamental frequencies, calculated by the nonlocal elasticity theory with the ones obtained from the MD simulations (i.e. norm of absolute error), is minimized. μ is set as optimization variable for the nonlocal elasticity theory. It should be noted that in the present work, relative error is employed instead of absolute error to get more realistic results. Table 5. shows the values of μ obtained in this paper using this nonlinear least square method for the SSSS, CCCC, and SCSC boundary conditions. Moreover, results compared with those suggested by Ansari et al. [10]. Appropriate value of μ for SCSC Boundaries

proposed for the first time, in this paper. It can be noted that as expected value of μ for SCSC graphene sheets lies between the ones corresponding to SSSS and CCCC.

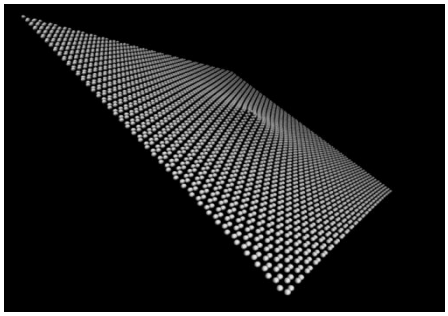

Fig.7
Excitation of first mode shape in the SLGS $(a = 10\ nm)$.

Table 4
Natural frequencies (THz) using MD simulations (LAMMPS).

Side lengths (*nm*)	SSSS	CCCC	SCSC
5	0.190430	0.351563	0.283203
10	0.061035	0.104980	0.090332
15	0.026855	0.051270	0.043945
20	0.017090	0.028076	0.023193
25	0.009766	0.019531	0.015869
30	0.007324	0.013428	0.012207

Table 5
The nonlocal parameter values for isotropic SLGS.

Boundary conditions	Isotropic (Present)	Isotropic [10]
SSSS	1.17	1.41
CCCC	0.86	0.87
SCSC	0.92	-*

The first natural frequencies of SSSS, CCCC, and SCSC Single layered isotropic graphene sheets, which are obtained using the nonlocal elasticity for evaluated values of μ, were compared in Fig. 8. It can be seen that for equal side lengths CCCC graphene sheets have higher natural frequency than SSSS graphene sheets. The natural frequency for SCSC graphene sheets is between those of SSSS and CCCC graphene sheets. Consequently, one can conclude that stronger constrains lead to higher natural frequency in graphene sheets. Lastly, Fig. 9, Fig. 10, and Fig. 11 display results gathered for the SLGSs based on the nonlocal elasticity using the isotropic properties and MD simulations for SSSS, CCCC, and SCSC boundary conditions, respectively. As shown in these figures the fundamental frequencies calculated by the isotropic assumption are in good agreement with results obtained by MD simulations. As a result, suggested values for the nonlocal parameters corresponding to SLGSs with various boundary conditions can yield satisfactory results.

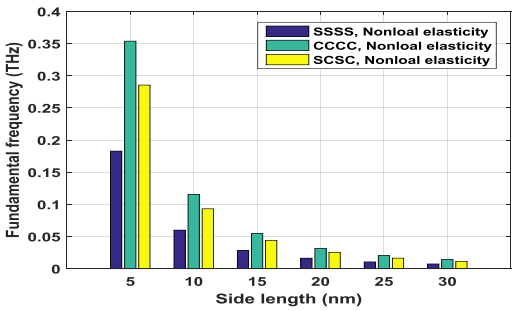

Fig.8
Comparison of the fundamental frequencies of SLGSs for various boundary conditions.

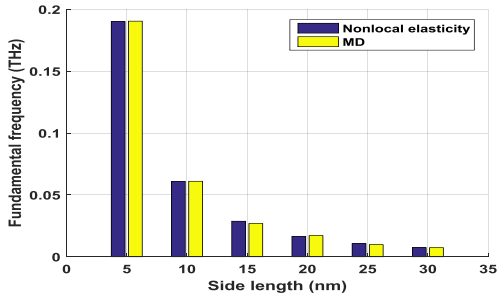

Fig.9
Comparison of the fundamental frequencies of SLGSs with SSSS boundaries for different methods.

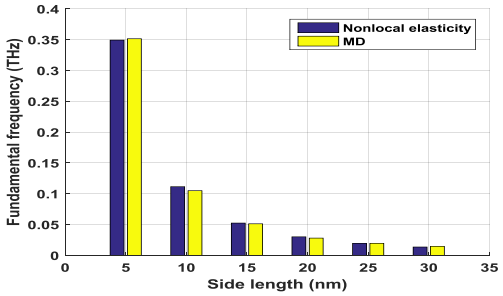

Fig.10
Comparison of the fundamental frequencies of SLGSs with CCCC boundaries for different methods.

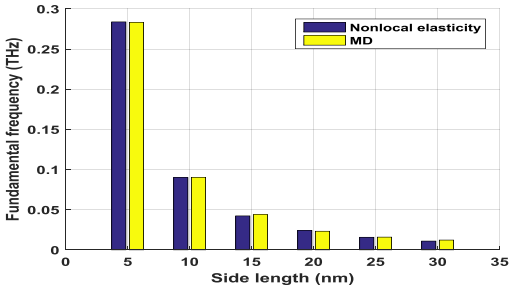

Fig.11
Comparison of the fundamental frequencies of SLGSs with SCSC boundaries for different methods.

6 CONCLUSIONS

A free vibration analysis of single-layered graphene sheets is performed using the nonlocal elasticity theory and the molecular dynamics simulations. The fundamental frequencies obtained by nonlocal elasticity theory are in good agreement with those reported in the literature. As expected, it was noted that graphene sheets with more rigid boundaries have higher natural frequencies. Moreover, the impact of the nonlocal parameter on the fundamental frequencies was observed. It was shown that in small scales the nonlocal parameter has a key role in determining the frequencies based on nonlocal elasticity theory. However, the effect of this parameter decreases as the size of graphene sheet increases.

Moreover, for the first time, the appropriate values of the nonlocal parameter were suggested in this work for isotropic graphene sheets with various boundary conditions including, CCCC, SSSS, and SCSC boundary conditions. It was shown that nonlocal elasticity theory can estimate the natural frequencies obtained by molecular dynamics simulation with good accuracy using these values.

REFERENCES

[1] Ramsden J., 2011, *Nanotechnology: An Introduction*, Elsevier.
[2] Murmu T., Pradhan S.C., 2009, Small-scale effect on the free in-plane vibration of nano plates by nonlocal continuum model, *Physica E: Low-Dimensional Systems and Nanostructures* **41**(8): 1628-1633.

[3] Baughman R.H., Zakhidov A.A., De Heer W.A., 2002, Carbon nanotubes-the route toward applications, *Science* 297(5582): 787-792.
[4] Liew K.M., Zhang Y., Zhang L.W., 2017, Nonlocal elasticity theory for graphene modeling and simulation: prospects and challenges, *Journal of Modeling in Mechanics and Materials* **1**(1): 0159.
[5] Pradhan S.C., Phadikar J.K., 2009, Nonlocal elasticity theory for vibration of nano plates, *Journal of Sound and Vibration* **325**(1): 206-223.
[6] Hosseini-Hashemi S., Zare M., Nazemnezhad R., 2013, An exact analytical approach for free vibration of Mindlin rectangular nano-plates via nonlocal elasticity, *Composite Structures* **100**: 290-299.
[7] Zhang Y., Lei Z.X., Zhang L.W., Liew K.M., Yu J.L., 2015, Nonlocal continuum model for vibration of single-layered graphene sheets based on the element-free kp-Ritz method, *Engineering Analysis with Boundary Elements* **56**: 90-97.
[8] Zhang Y., Zhang L.W., Liew K.M., Yu J.L., 2016, Free vibration analysis of bilayer graphene sheets subjected to in-plane magnetic fields, *Composite Structures* **144**: 86-95.
[9] Ansari R., Rajabiehfard R., Arash B., 2010, Nonlocal finite element model for vibrations of embedded multi-layered graphene sheets, *Computational Materials Science* **49**(4): 831-838.
[10] Ansari R., Sahmani S., Arash B., 2010, Nonlocal plate model for free vibrations of single-layered graphene sheets, *Physics Letters A* **375**(1): 53-62.
[11] Pradhan S.C., Kumar A., 2011, Vibration analysis of orthotropic graphene sheets using nonlocal elasticity theory and differential quadrature method, *Composite Structures* **93**(2): 774-779.
[12] Xing Y.F., Liu B., 2009, New exact solutions for free vibrations of thin orthotropic rectangular plates, *Composite Structures* **89**(4): 567-574.
[13] Setoodeh A.R., Malekzadeh P., Vosoughi A.R., 2011, Nonlinear free vibration of orthotropic graphene sheets using nonlocal Mindlin plate theory, *Proceedings of the Institution of Mechanical Engineers, Part C: Journal of Mechanical Engineering Science*.
[14] Shahidi A.R., Shahidi S.H., Anjomshoae A., Estabragh E.R., 2016, Vibration analysis of orthotropic triangular nano plates using nonlocal elasticity theory and Galerkin method, *Journal of Solid Mechanics* **8**(3): 679-692.
[15] Zhang L.W., Zhang Y., Liew K.M., 2017, Modeling of nonlinear vibration of graphene sheets using a mesh free method based on nonlocal elasticity theory, *Applied Mathematical Modelling* **49**: 691-704.
[16] Eringen A.C., 1983, On differential equations of nonlocal elasticity and solutions of screw dislocation and surface waves, *Journal of Applied Physics* **54**(9): 4703-4710.
[17] Reddy J.N., Phan N.D., 1985, Stability and vibration of isotropic, orthotropic and laminated plates according to a higher-order shear deformation theory, *Journal of Sound and Vibration* **98**(2): 157-170.
[18] Reddy J.N., 2004, *Mechanics of Laminated Composite Plates and Shells: Theory and Analysis*, CRC press.
[19] Bert C.W., Malik M., 1996, Differential quadrature method in computational mechanics: a review, *Applied Mechanics Reviews* **49**: 1-28.
[20] Plimpton S., 1995, Fast parallel algorithms for short-range molecular dynamics, *Journal of Computational Physics* **117**(1): 1-19.
[21] Haile J.M., Johnston I., Mallinckrodt A.J., McKay S., 1993, Molecular dynamics simulation: elementary methods, *Computers in Physics* **7**(6): 625-625.
[22] http://lammps.sandia.gov/doc/Manual.html/, Sandia National Laboratories, 2015.
[23] Seifoori S., Hajabdollahi H., 2015, Impact behavior of single-layered graphene sheets based on analytical model and molecular dynamics simulation, *Applied Surface Science* **351**: 565-572.
[24] Chu E., 2008, *Discrete and Continuous Fourier Transforms: Analysis, Applications and Fast Algorithms*, CRC Press.
[25] Sakhaee-Pour A., 2009, Elastic properties of single-layered graphene sheet, *Solid State Communications* **149**(1): 91-95.